JOURNAL OF THERMOPHYSICS AND HEAT TRANSFER
Vol. 19, No. 4, October–December 2005

Two-Phase Zero-Gravity Pressure-Drop Predictions from Single-Phase One-*g* Data

Ken Marsden*
Argonne National Laboratory-West, Scoville, Idaho 83415
and
Cable Kurwitz† and Frederick Best‡
Texas A&M University, College Station, Texas 77843-3133

The purpose of this work was to use a single-component, R-12, two-phase flow test loop to produce and collect pressure-drop data from the corrugated tubes and quick-disconnect components and develop correlations and prediction methods for two-phase pressure drops in normal and reduced gravity. Results show it is possible to predict the zero-gravity pressure drops through the corrugated tubes using the homogeneous equilibrium model and single-phase, ground-based pressure-drop measurements. It was also found that prediction of pressure drop through the quick-disconnect attachment could be obtained using the homogeneous equilibrium model (with single-phase ground-based measurements) coupled with an orifice pressure drop model. The use of single-phase, ground-based experiments to predict two-phase, reduced gravity component performance could yield significant cost savings and increased reliability of reduced gravity fluid systems.

Introduction and Background

INCREASED knowledge of zero-gravity two-phase flow phenomenology would be beneficial for future space exploration. Two-phase flows are inherent in proposed space systems such as advanced life support, high-performance thermal management systems and power conversion systems. The latter is of interest to NASA in regard to Project Prometheus, the development of nuclear-powered exploration spacecraft. Rankine cycles currently are currently being investigated by NASA and Oak Ridge National Laboratory for use in nuclear power systems.[1] Rankine cycles are particularly attractive above 50 kW(e) but are limited by two-phase flow issues.[2]

Two-phase flow system performance is better than single-phase systems in that two-phase flow can provide enhanced system performance through significant reductions in volume, mass, and power requirements.[3] Further, higher power per unit mass can be transported using smaller heat exchange components. Design of a two-phase system for reduced gravity requires determination of the optimum thermodynamic state points as well as various specialized component information (i.e., flow regime pressure drop). A growing body of research regarding two-phase flow under reduced gravity conditions is becoming available; however, most research deals with idealized conditions such as straight pipes rather than components that are typically used to fabricate actual fluid systems such as tees, valves, quick disconnects, etc. The following paper investigates experimental pressure drop results for components originally intended for use in a two-phase thermal management system on Space Station *Alpha*. Although the United States no longer plans to include a two-phase system on its portion of the International Space Station, these components can be utilized in proposed space nuclear-power systems.

Received 18 June 2004; revision received 30 December 2004; accepted for publication 17 January 2005.

*Technology Development Engineer, Building 713; ken.marsden@anl.gov.
†Senior Research Engineer, Department of Nuclear Engineering; kurwitz@tamu.edu.
‡Associate Professor, Department of Nuclear Engineering; fbest@tamu.edu.

Early reduced-gravity experimenters[4–9] studied two-phase liquid/vapor mercury flow for use in a Rankine power cycle as part of the Space Nuclear Auxilary Power (SNAP) program. They found the Lockhart–Martinelli correlation predicted pressure drops in the high-quality region within 70% and the low quality within 200%. Overall, they noticed little difference between 1-*g* and reduced-gravity pressure drops. However, testing was conducted primarily in the mist-flow regime. The high-quality regime is friction dominated, for which gravity would have a minor effect as demonstrated by the quality dependence on the accuracy of the pressure-drop prediction. Differences between 0 and 1-*g* pressure drop were published in 1975 by Heppner et al.[10] Pressure-drop data for air/water in plastic tubes indicated higher pressure drops in reduced gravity for the same flow conditions compared with ground tests. A quantitative study of the pressure-drop data was not included, but the authors concluded that gravity influences pressure drop because it influences flow regime. In 1987, other researchers[11,12] reported pressure-drop and flow-regime data for an R114 two-phase loop flown on the NASA/JSC KC-135. Flow regimes included slug and annular flows for reduced gravity and stratified and annular flows on the ground. Observed pressure drops were found to be generally 20% higher in reduced gravity than 1 *g*. However, the low sensitivity of the differential pressure transducer led to large uncertainties at low pressure drops.

Lambert[13] studied pressure-drop data from a previous version of the experiment package used in this paper. She suggested modeling approaches for the annular (separated), slug, and bubbly (homogeneous) regimes as well as developing a methodology to correct the experimental data for residual aircraft acceleration and instrumentation effects. She found that these corrections could be significant, which is important because almost all two-phase reduced-gravity testing has been conducted on aircraft flying parabolic trajectories where the duration of low gravity is on the order of 20 s and residual accelerations on the order of 0.01 *g* (Ref. 14). Further research using the same experiment package as Lambert found most reduced-gravity flows to be reasonably predicted by the separated flow model, and they found the homogeneous equilibrium model (HEM) adequate for bubbly/slug flow conditions.[15] In 1992, Wheeler[16] developed a model describing smooth annular flows for smooth tubing obtained with the same package used to collect the data used in this paper. He used the universal velocity profile to estimate film thickness, and his interfacial shear correlation predicted most of the data well. Although Wheeler's method for smooth annular flows shows good agreement with smooth tubing, it is highly improbable that it would accurately model corrugated flexible hose. A flow-regime model derived from a database of all

reduced-gravity flow-regime data in the open literature including results from the tests described in this paper up to 1993 was completed by Reinarts.[17] A flow-regime transition model using a force-balance approach was presented. In 1993, Miller et al.[18] published an analysis of reduced-gravity pressure drops in the two sizes of smooth glass tubing used in this package and found that the Troniewski and Ulbrich prediction and the Lockhart–Martinelli/Chisholm prediction both correlate well with the experimental pressure drops. They found that the HEM and smooth annular prediction generally underpredicted their data. Data reported by Lambert, Hill and Best, Wheeler, and Reinarts (Refs. 13, 15–17) revealed higher pressure drops for reduced-gravity than 1-g horizontal flow conditions.

Nishikawa et al.[19] published a paper on vertical, air-water annular flow in transverse square-grooved tubes under 1 g. Tubes had diameters near 25 mm with groove depths of 0.5 and 1.0 mm and a pitch of 4 mm. Corrugated flexible hoses in this paper have diameters between 8 and 15 mm with rounded groove depths and pitches near 3 mm. The authors found the single-phase friction factor of the wall to be significantly less than that predicted by the macroscopic roughness ε/D. A review of the results indicates that flowing fluid does not penetrate into the groove depth, which is important because the present work has components with large corrugation depths. They also observed an increase in entrainment with increasing roughness. This should increase the friction pressure drop and make the flow more homogeneous.

Previous components studied under 1-g two-phase flow conditions included a quick-disconnect prototype similar to but larger in size to that evaluated herein.[20] The maximum pressure drop across the quick-disconnect prototype at 13 g/s liquid flow and 16 g/s vapor flow was approximately 200 Pa. Unfortunately, this was near the accuracy of the transducer; in addition, the authors did not provide form loss predictions or provide specific dimensions of the quick-disconnect prototype used. Although their results are interesting, they are not directly applicable to this work because of the lack of specific details regarding the device.

One of the better known methods for determining the pressure drop through orifices and venturis similar to the internals of the quick-disconnect presented here assumes that slip equals one and that the fluid behaves as an incompressible fluid through the orifice.[21] The method simplifies to

$$\Delta P_{\mathrm{TP}}/\Delta P_L = 1 + C(\Delta P_V/\Delta P_L)^{0.5} + \Delta P_V/\Delta P_L \qquad (1)$$

where $C = Z + (1/Z)$, with $Z = (\rho_l/\rho_v)^{1/2}$. ΔP_1 and ΔP_v are the pressure drops for the liquid and vapor phase traveling alone through the orifice and ΔP_{TP} is the two-phase pressure drop.

Three devices are analyzed in this paper; two are different sizes of corrugated flexible hose, and the third is a quick-disconnect device. Complex two-phase thermal management systems for a spacecraft could require the capability to be assembled on orbit or to facilitate removal and replacement of critical components. For this purpose, it is envisioned that short lengths of flexible hose and a quick-disconnect fitting would be placed at the end of each section of tubing. It is then simple for astronauts to snap together appropriate lines. The quick-disconnect fitting is designed to be nonleaking, constant volume, and relatively simple to connect or disconnect. The nonleaking criterion is important to prevent the escape of potentially hazardous fluids that might be carried into a living space on the astronaut's suit.

The project that collected the component experimental data in this paper was primarily intended to produce a reduced-gravity database of flow-regime and pressure-drop information through smooth tubes for use in designing two-phase thermal management systems for reduced gravity (i.e., Ref. 16). Because the experiment package had two test sections, modifications were made to the second test section, and the opportunity was taken to fly two sizes of corrugated hose and the quick-disconnect model.[22] The intent of this paper is to provide an analysis and modeling of the pressure drop through the aforementioned components for potential design use.

Experimental Methods

Experimental Environment

The data collected for this paper were obtained using a two-phase flow test package flown on the NASA Johnson Space Center KC-135A aircraft stationed at Ellington Field in Houston, Texas. This aircraft produces alternating periods of low and high gravity by flying a parabolic path. During these experiments, three parabolas were flown in series, with 1–2 min of level flight between sets of the three parabolas. Although the low acceleration conditions produced on the KC-135 are commonly described as microgravity, they are actually characterized by vertical accelerations in the hundredths of g range. For this paper, the period of low acceleration is termed reduced gravity.

The accelerations are measured in a triaxial coordinate system. For this coordinate system, the x axis is parallel to the transverse axis of the plane with the positive direction pointing to the left when facing forward toward cockpit, the y axis is parallel to the longitudinal axis of the plane with the positive direction pointing towards the rear of the aircraft, and the z axis is perpendicular to the deck with the positive direction pointing toward the ceiling. The test-section axial direction is mounted parallel to the x axis. An overall analysis was done of the acceleration conditions during most of the 19 flights (approximately 800 parabolas) with the flow loop on the KC-135. The reduced gravity produced by the aircraft is typically 18.6 ± 1.9 s in duration followed by a high-g pullout of 43 ± 6 s in length. The transition time from the high g into an acceleration less than 0.05 g requires 5.6 ± 1.3 s. The reduced-gravity periods were found to have an average vertical acceleration of $+0.008 \pm 0.021$ g, and the pullouts had an acceleration of 1.6 ± 0.2 g. The rapid transitions in vertical acceleration are coupled with smaller acceleration transients in Gy. Figure 1 shows triaxial acceleration for three typical parabolas. A 0.1 to 0.2 g peak can be seen in Gy preceding the reduced-gravity period. This acceleration is from the maneuvering of the aircraft. Although Gy during the reduced-gravity period is slightly smoother than Gx, the experiment package had its test sections aligned in the x direction, perpendicular to the aircraft fuselage. This is because of concerns about sloshing and nonequilibrium introduced from the Gy peaks preceding the reduced gravity. Figure 2 shows the acceleration values in a typical reduced gravity period.[14]

Experiment Test Facility

Figure 3 shows the Foster-Miller/Air Force–Phillips Laboratory two-phase flow experiment package that flew aboard the KC-135 and produced the data in this paper. An important feature of this package is its two-phase pump. The two-phase pump separates a mixture into single-phase constituents and independently increases the pressure of each phase. The vapor and liquid flow rates are independently set by metering valves at the pump outlets. This enables accurate mass flow measurement of the separated liquid and vapor streams.

Sequentially, in the two-phase flow loop, the flow stream begins with the two-phase pump, where the gas/liquid Freon R12 is separated and the pressure head of each phase increased. For each

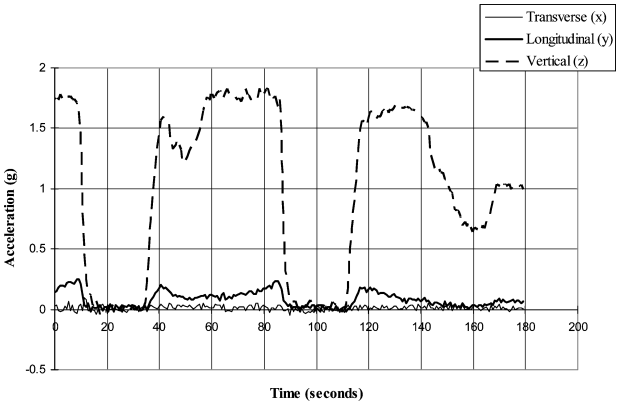

Fig. 1 Typical acceleration environment on the KC-135.

phase, two parallel measurement sections are used to monitor flow rates. The vapor flow stream utilizes Fox venturis in combination with Validyne pressure transducers. The liquid stream employs a bearingless-type flowmeter for flow conditions above 5 g/s and a paddle-wheel type flowmeter for liquid flows below 5 g/s. To allow for the change in liquid volume in the flow loop, a liquid accumulator is located at the pump liquid outlet.

The gas and liquid are mixed, and the fluid mixture then travels through a smooth 90-deg bend, through a variable length developing section, and into the first of two test sections. The first test section is made up of a glass tube of similar diameter to the development length. The clear adiabatic test section allows the flow regime to be recorded via a high-speed digital imaging system. The second test section had special fittings allowing corrugated flexible hose, quick-disconnect components, or glass tubing to be inserted. Differential pressure measurements for both test sections are made with a pair of Foxboro 823 electronic ΔP cell transmitters. The adiabatic test sections are each 1.25 m long. More detailed system descriptions can be found in Marsden[22] and Wheeler.[16]

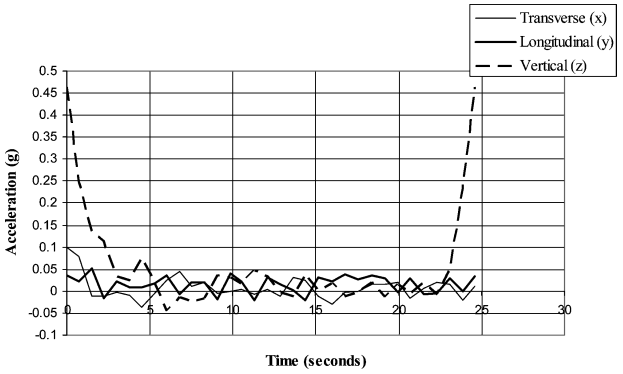

Fig. 2 Reduced-gravity acceleration environment on the KC-135.

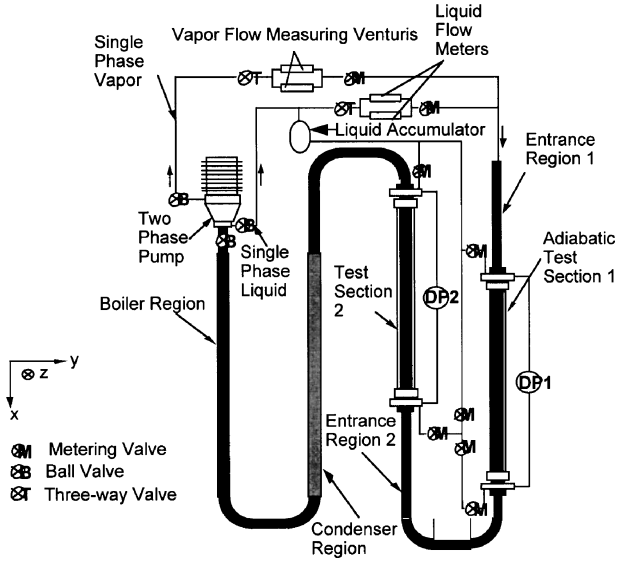

Fig. 3 Foster-Miller/Air Force–Phillips Laboratory two-phase flow package.

Experiment Components

Three components in the second test section of the experiment package are the subject of this paper. Two components are corrugated flexible hose sections. These corrugated hose test sections were preceded by an approximately 45 cm developing length (of identical corrugated hose) and have characteristics as described in Table 1. Figure 4 is a schematic of the large and small corrugated hoses. This developing length provides for approximately 33 and 58 lengths over diameters (LDs) for the large and small corrugated hose, respectively.

The quick-disconnect (QD) component was preceded by approximately 60 cm of stainless-steel smooth tube developing length. This is approximately 55 L/Ds. After the first pressure tap, a 7.6-cm smooth tube led into the 16.5-cm-long QD prototype. Following the prototype is a 32.0 cm length of corrugated hose and then 56.4 cm of smooth glass tube before the second pressure tap. The dimensions of the pieces are shown in Table 2, and the schematic of the whole component is shown in Fig. 5 and a picture in Fig. 6.

Table 1 Corrugated hose dimensions

	Dimensions of corrugated hose			
Component	Length, cm	Min. internal diameter, cm	Corrugation depth, cm	Corrugation pitch, cm
Large corrugated hose	124.5	1.38	0.45	0.36
Small corrugated hose	124.5	0.77	0.30	0.31

Table 2 Quick disconnect dimensions

	Dimensions of quick-disconnect components			
Component	Length, cm	Min. internal diameter, cm	Corrugation depth, cm	Corrugation pitch, cm
Stainless-steel tubing	60	1.09	N/A	N/A
Medium corrugated hose	32	12.95	0.35	0.36
Smooth glass	56.4	1.05	N/A	N/A

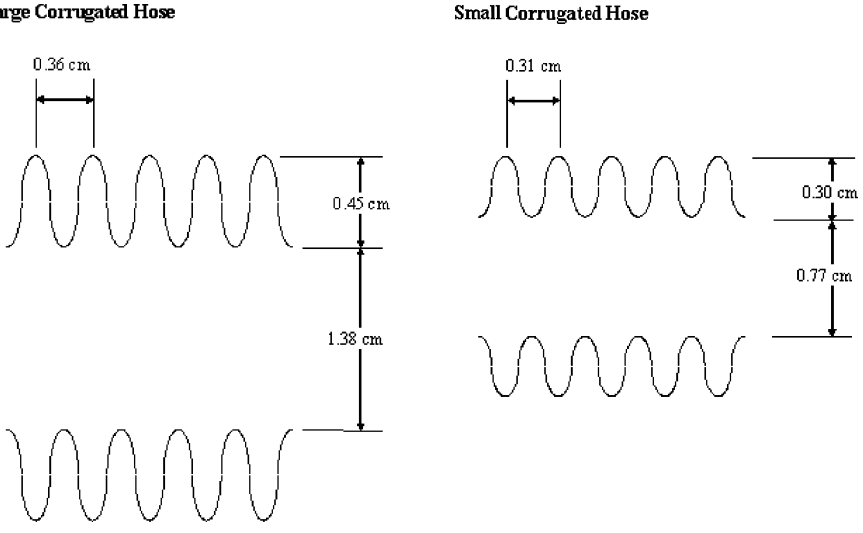

Fig. 4 Corrugated flexible hose dimensions.

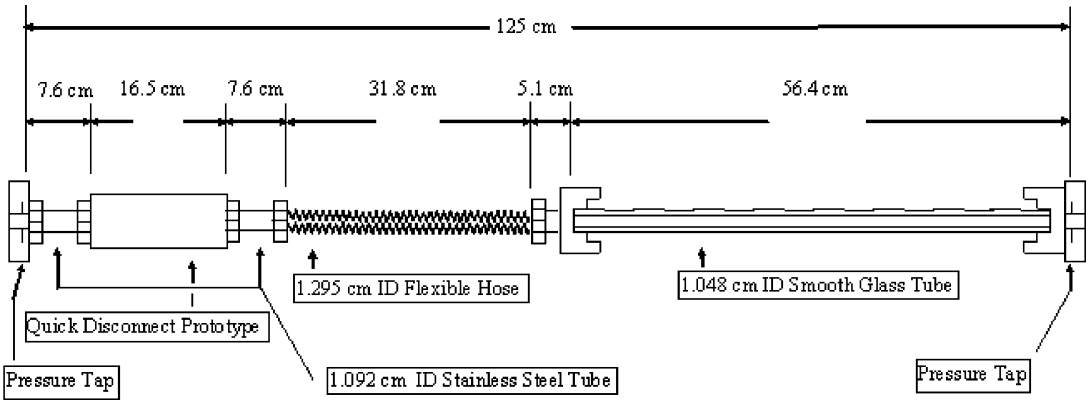

Fig. 5 Quick-disconnect setup.

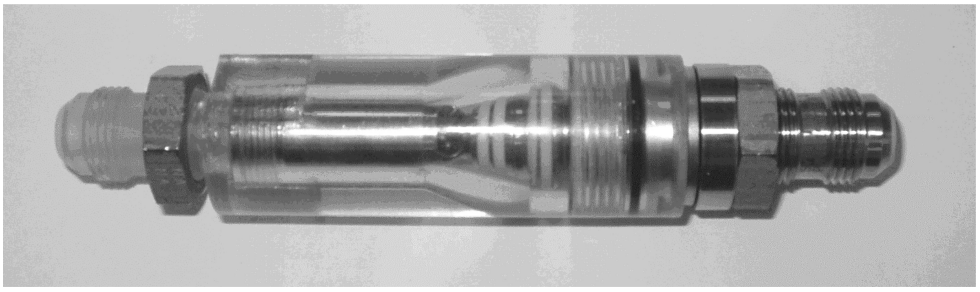

Fig. 6 Quick-disconnect picture.

The behaviors of the vapor flow transducers were tested in a scoping experiment on a previous flight in the aircraft to determine their acceleration sensitivity.[23] The KC-135 environment has a negligible effect on the differential pressure sensor when the diaphragm is oriented normal to the x axis of the aircraft; this is the orientation used for the experiment package. Accuracy for the flow measurement is as follows[24]:

1) Low-vapor-flow transducer: ±5% for the range 1.0 to 3.0 g/s.

2) Low-vapor-flow transducer: ±0.1 g/s for the range 1.0 to 0.1 g/s.

3) High-vapor-flow transducer: ±5% for the range 2.0 to 11.0 g/s.

4) Low- and high-liquid-flow transducers: ±5% for the full range.

A paddle-type differential pressure transducer was utilized for the ΔP measurement. The transducer utilized large sensing diaphragms that displaced silicone oil connected to the remote displacement sensor. The fluid interface diaphragm region is shown in Fig. 7. This schematic shows the region as it was for the glass sections in test section one. Flow travels through the glass test section into the stainless-steel tube. The fluid cavity next to the pressure paddle diaphragm communicates with the flow path via the pressure-sensing path and four small wall taps. The silicone-filled pressure line travels from the pressure paddle diaphragm to the transducer. The transmitters were calibrated over the range 0 to 20 kPa with an accuracy of 50 Pa differential. For the quick-disconnect component, the connection was smooth so form pressure drops should be minimal. The large corrugated hose had a small amount of mismatch in the connection. Estimates of the magnitude of induced error indicate it should not have more than 5%. The standard error for these pressure drops is large enough so that this uncertainty was neglected. The small corrugated hose had a one-step flow-path area decrease at the outlet where the 7.7-mm glass met a 5.0-mm steel tube. This flow-path diameter change and the resulting flow acceleration could have increased measured pressure-drop by as much as 50%. For this reason, the small corrugated hose measured pressure-drop data should be considered an upper limit to the true pressure drop.

All uncertainties listed in this paper are computed using standard error. The calculation for standard error is

$$\sigma = \sqrt{\sigma_{\text{std}}^2 + \sigma_{\text{DA}}^2 + \sigma_{\text{inst}}^2} \tag{2}$$

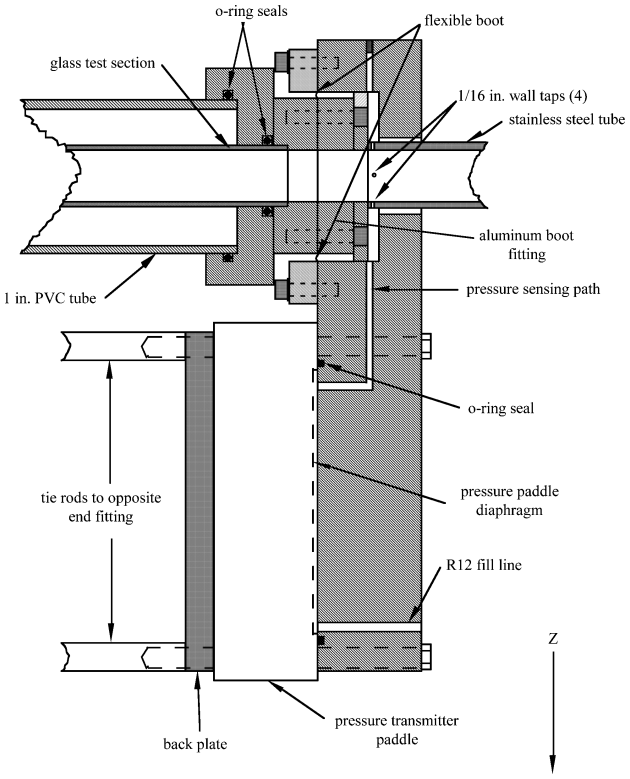

Fig. 7 Pressure paddle/test-fluid Interface region.

where σ_{std} is the standard deviation of the measurement, σ_{DA} is the error from the digital acquisition system, and σ_{inst} is the instrument error.

Data Rejection Criteria

An original test condition was defined as follows. A limit of $|0.05|g$ was applied to the acceleration in each direction, and each reduced gravity period had to have a minimum of nine consecutive

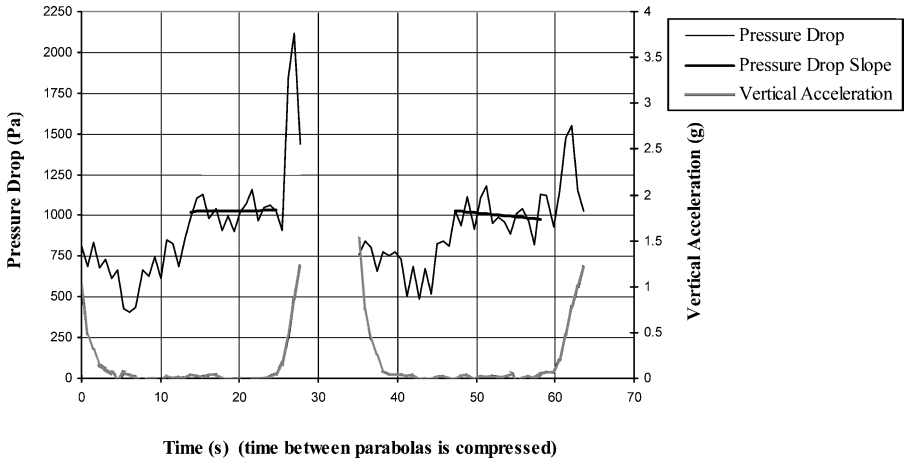

Fig. 8 Example of pressure-drop slope for equilibrium determination.

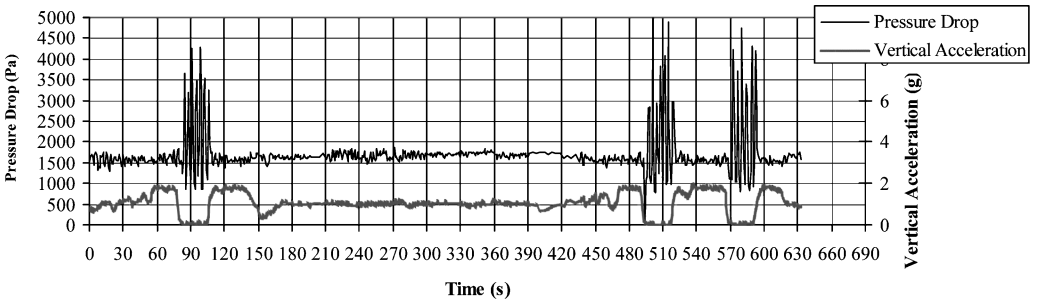

Fig. 9 Pressure drop for parabolas with large fluctuations (8/19/91 ITP 5).

readings a 1 Hz within $|0.05|g$ or it would be excluded. Data exceeding the acceleration limit and failing to meet the time interval were excluded. To be conservative, one cycle of acceleration data collected before and after readings in excess of the specified limit was removed.

Because the pressure drop is dependent upon the flow regime, equilibrium effects associated with the transition from high g to low g were analyzed. This effect is especially pronounced in the corrugated hose as the flow regime changes from stratified flow under 2 g to annular flow in reduced gravity. Stratified liquid is wicked into the previously empty corrugations (grooves) as the flow regime changes to annular under reduced gravity. Some parabolas indicate a time-varying pressure drop. However, many parabolas show an initial dip in pressure drop followed by a recovery to a relatively flat 'plateau' as the flow reached an equilibrium condition. Therefore, the first 7–10 s of data of the reduced gravity period are excluded when computing the average pressure drop. If an equilibrium plateau is reached after this point, the averaging begins at the start of the plateau. Quantitatively, a least-squares method was used to determine the slope of the pressure drop over the chosen time period of the plateau and then multiplied by the length of the line and divided by the average ΔP. The result shows the percentage increase or decrease in ΔP over the averaging period. If the change in magnitude was less than 10% over the length of the plateau (5–7 s), the parabola was accepted. For some test points, large fluctuations in the measured pressure drop make the slope measurement sensitive to beginning and ending points. The addition or exclusion of a particular data point significantly alters the slope. For these parabolas the slope criterion was ignored, and they were accepted.

Figure 8 shows pressure drop vs time for two typical parabolas. The initial decrease in pressure drop followed by a plateau is clearly visible. The slope of the plateau is also shown. Figure 9 shows a series of three parabolas where the standard deviation of the pressure drop during reduced gravity was very high. For these parabolas, the slope criterion was ignored. Each parabola must have an average pressure drop greater than 125 Pa. This is the practical lower limit of the pressure-drop measurement.

Mass flow rates for all of the data points were judged to be in equilibrium. Parabolas showing a vapor or liquid flow rate increasing or decreasing more than 20% during the reduced gravity period were eliminated. Care must be taken when evaluating the effect of measured flow rates on the system. Hysteresis effects on the system from rapid changes between 2 g and reduced gravity were observed infrequently. These effects on the flow rate were ignored because they most likely do not affect flow conditions in the second test section until after the reduced-gravity period. Minimum liquid flow rates that would allow the corrugated hoses to fill the empty corrugated grooves and come to an equilibrium during a parabola were determined. This calculation assumed that the tube contained stratified liquid up to the center of the tube. The minimum flow rate determined was 6.5 g/s for the large diameter corrugated hose and 5 g/s for the small diameter corrugated hose.

Data Analysis and Results

Single-Phase, Ground-Based Data

The resulting corrected pressure drops and flow conditions for flight testing are presented for each component along with corresponding results of the single-phase ground experiments. Figure 10 is a plot of the friction factor vs Reynolds number, which includes the experimental friction factor for single-phase liquid in the large corrugated hose and the quick-disconnect section.

The single-phase friction factors were computed using the well-known formula for head loss:

$$\Delta P = f(L/D)(\rho V^2/2) \tag{3}$$

These friction factors were computed using the known flow rates, tube dimensions, and measured pressure drops. The Colebrook–White formula[25]

$$1\Big/\sqrt{f} = 2 \cdot \log\left[(\varepsilon/D)/3.71 - 2.51\Big/Re\sqrt{f}\right] \tag{4}$$

is shown for the ε/D calculated for the large corrugated hose and quick-disconnect component. For the work presented herein, this

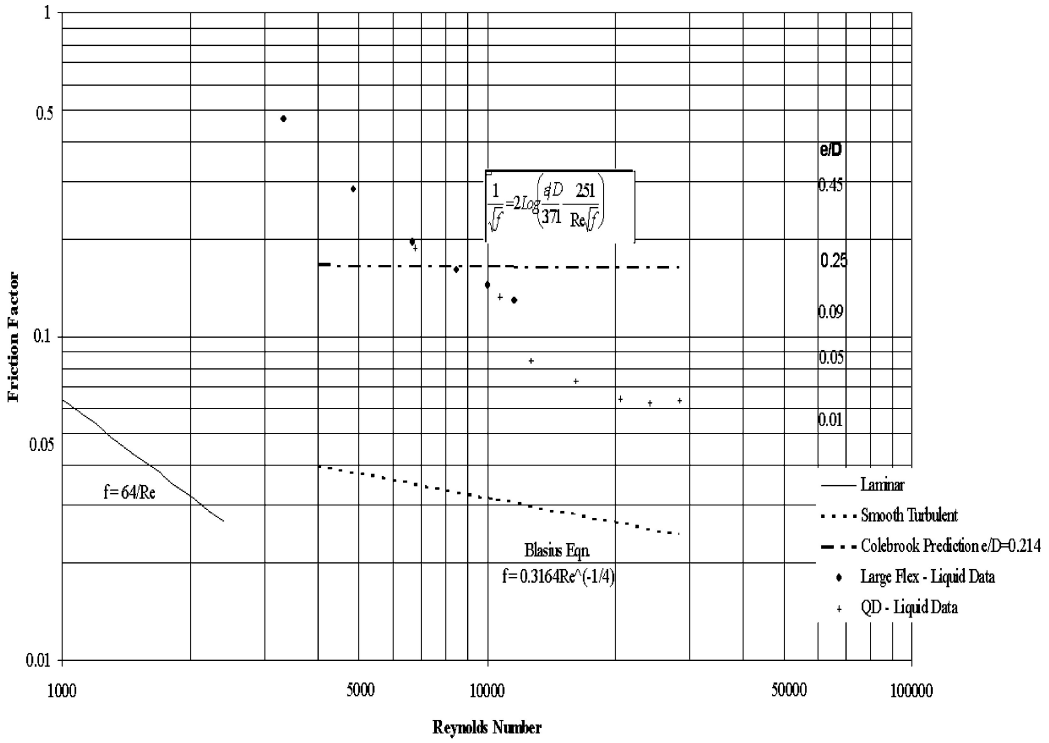

Fig. 10 Single-phase liquid tube friction factor vs Reynolds number.

equation applies when the laminar boundary layer δ is less than 1.7ε. The laminar boundary layer is calculated with the equation

$$\delta = 14.12\nu \Big/ V\sqrt{f} \tag{5}$$

where ν is the kinematic viscosity of the liquid and V is the bulk velocity.

With the corrugation depth as ε, the laminar boundary layer for all of the flows in this paper is significantly smaller than 1.7ε. The literature contains no description of the magnitude of roughness for which these equations apply, but most likely they were not intended for application to large, regular corrugations. The ε/D was computed using the corrugation depth and is 0.214 for the large corrugated hose and 0.3 for the quick-disconnect corrugated hose. Referring to the Moody diagram, for large values of ε/D the prediction of the friction factor asymptotically approach a constant value. The values of ε/D shown on the right side of Fig. 10 are the equilibrium values for the particular friction factor indicated on the left. It can be seen that the friction factors for both the large corrugated hose and the quick-disconnect component are a strong function of Reynolds number, whereas the Colebrook equation is not. The Colebrook equation is a function of Reynolds numbers where the nature of the flow interaction with the roughness is changing. At lower Reynolds numbers, the ratio ε/δ approaches unity, and the roughness actually protrudes into the turbulent core. Once this transition has occurred, the friction factor is relatively constant. For the components in this paper, phenomena different from this determine the effective friction factor. ε/D is obtained experimentally from single-phase testing in 1 g. These friction factors are presented because they are used in the prediction methods developed in the subsequent section.

Figure 11 is the Moody chart with the single-phase friction factors for the vapor flow plotted for the large corrugated hose and quick-disconnect component.

Two-Phase Reduced-Gravity Data

In addition to the single-phase, 1-g pressure-drop data, a significant quantity of two-phase, reduced-gravity pressure-drop data was collected. All of the flight data for these components are two phase. Data for all parabolas flown with the three components can be found by Marsden.[22] Table 3 shows the 24 acceptable, corrected pressure-drop data points for the large corrugated hose. The system temperature for all of these parabolas is between 290 and 301 K. Parabolas with ΔP fluctuation in the comments section had significant fluctuations in pressure drop that made the equilibrium calculation extremely sensitive to beginning and ending points as explained earlier. Table 4 shows the eight acceptable data points for the small corrugated hose, and Table 5 lists the 13 acceptable data points for the quick-disconnect component.

Pressure-Drop Modeling

The pressure-drop modeling of the large and small corrugated flexible hoses consists of utilizing the HEM and loss coefficient developed from single-phase ground testing. This method can be used to predict two-phase pressure drop under reduced-gravity conditions through the corrugated hoses. A different modeling approach is utilized to model the pressure drop through the quick disconnect. Two methods were evaluated: 1) an orifice model based on the work done by Chisholm that is applied to the entire device and 2) a split-component model that breaks the quick disconnect into sections. Modeling the quick disconnect as split sections and using the HEM prediction for the corrugated flexible hoses provides good predictions of 0-g two-phase pressure drop using single-phase, 1-g data. These methods are very valuable in cost savings and increased reliability of two-phase space systems using only inexpensive ground testing.

Homogeneous Equilibrium Model

The foundation of the pressure-drop prediction method used is the HEM. This model assumes well-mixed vapor and liquid moving at identical average velocities. Because of its assumptions, this prediction method works best for well-mixed and homogeneous-type flows and is well suited for the geometry of the system under evaluation. The standard form of the equation is

$$\Delta P = (f_{\mathrm{TP}}/D)\left(G^2 \Big/ 2\rho_m\right) \tag{6}$$

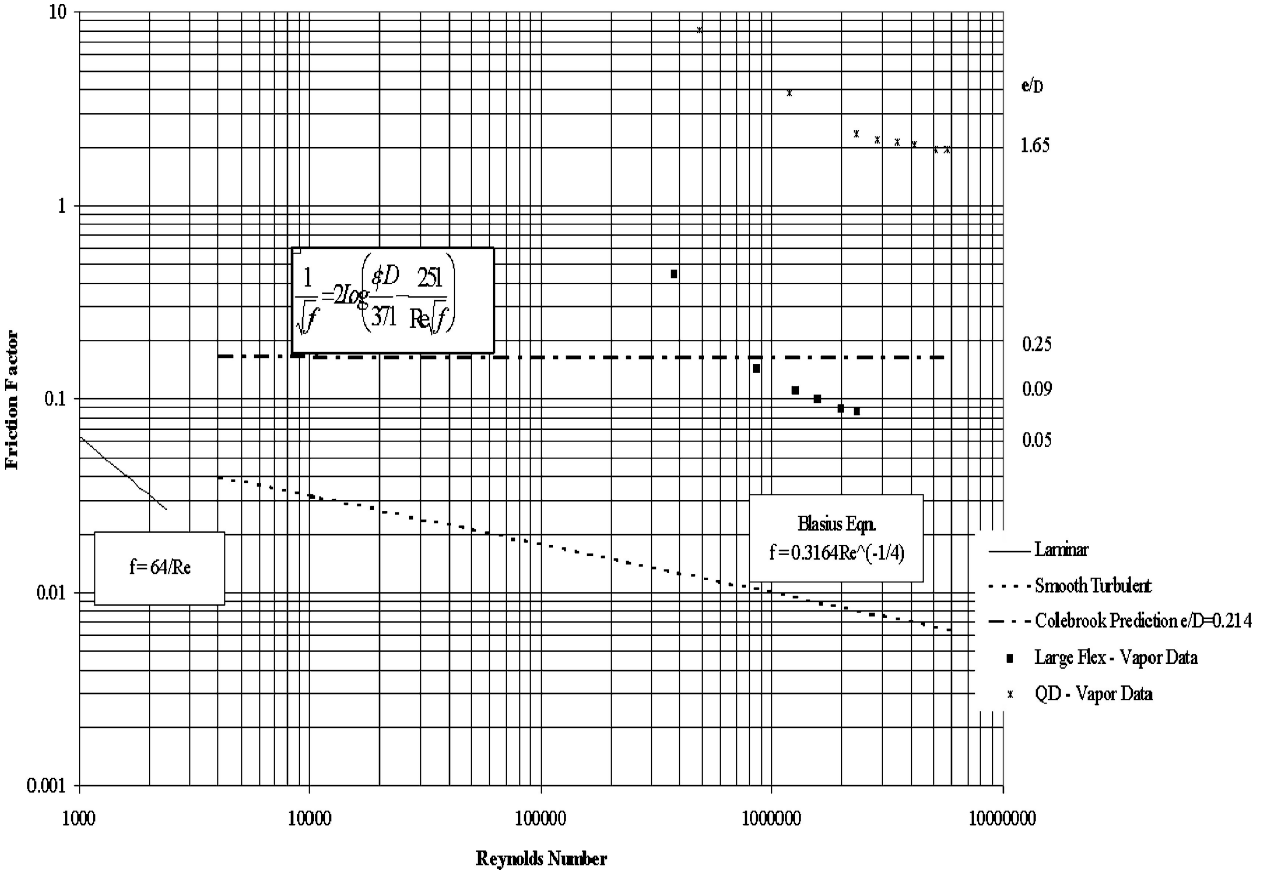

Fig. 11 Single-phase friction factors for large corrugated hose and quick disconnect.

Table 3 Two-phase, reduced-gravity data listing for large corrugated tube

Data point	Vapor flow, g/s	Liquid flow, g/s	ΔP, Pa	Comments
1	1.5 ± 0.4	19.3 ± 1.6	280 ± 97	OK
2	6.5 ± 0.4	23.0 ± 2.3	1087 ± 108	OK
3	1.9 ± 0.3	11.6 ± 0.8	197 ± 95	OK
4	11.7 ± 0.6	11.2 ± 0.7	2163 ± 1247	OK, ΔP fluctuations
5	11.8 ± 0.7	10.8 ± 0.7	2201 ± 1300	OK, ΔP fluctuations
6	11.7 ± 0.7	10.8 ± 0.6	2174 ± 1131	OK, ΔP fluctuations
7	9.8 ± 0.6	20.0 ± 1.6	2430 ± 982	OK
8	4.5 ± 0.3	7.3 ± 0.5	244 ± 97	OK
9	4.5 ± 0.3	6.8 ± 0.6	319 ± 72	OK
10	4.4 ± 0.3	7.2 ± 0.5	357 ± 70	OK
11	8.9 ± 0.5	7.8 ± 0.5	1017 ± 88	OK
12	8.9 ± 0.5	7.8 ± 0.6	994 ± 112	OK
13	9.0 ± 0.5	7.8 ± 0.5	983 ± 82	OK
14	1.8 ± 0.1	18.3 ± 1.2	378 ± 57	OK
15	1.8 ± 0.1	18.4 ± 1.1	309 ± 64	OK
16	1.8 ± 0.1	18.5 ± 1.1	336 ± 68	OK
17	1.8 ± 0.1	42.9 ± 2.2	960 ± 81	OK
18	1.1 ± 0.1	20.7 ± 1.4	177 ± 85	OK, ΔP fluctuations
19	2.7 ± 0.2	45.0 ± 2.9	1655 ± 78	OK
20	2.6 ± 0.2	45.4 ± 2.4	1628 ± 101	OK
21	2.6 ± 0.2	45.4 ± 2.4	1611 ± 72	OK
22	9.0 ± 0.6	10.7 ± 0.8	1516 ± 348	OK, ΔP fluctuations
23	8.9 ± 0.6	10.9 ± 0.8	1497 ± 403	OK, ΔP fluctuations
24	8.9 ± 0.7	10.6 ± 0.7	1478 ± 481	OK, ΔP fluctuations

Table 4 Two-phase, reduced-gravity data listing for small corrugated tube

Date	Vapor flow, g/s	Liquid flow, g/s	ΔP, Pa	Comments
25	1.4 ± 0.2	9.5 ± 0.8	2232 ± 120	OK
26	1.5 ± 0.1	9.7 ± 0.6	2201 ± 105	OK
27	1.5 ± 0.2	9.7 ± 0.7	2256 ± 117	OK
28	1.5 ± 0.2	9.3 ± 0.7	2248 ± 91	OK
29	1.5 ± 0.2	9.6 ± 0.8	2282 ± 94	OK
30	2.3 ± 0.2	7.2 ± 0.6	2505 ± 72	OK
31	2.3 ± 0.1	7.1 ± 0.7	2500 ± 112	OK
32	1.6 ± 0.2	5.9 ± 0.5	1311 ± 75	OK

Table 5 Two-phase, reduced-gravity data listingfor quick disconnect

Date	Vapor flow, g/s	Liquid flow, g/s	ΔP, Pa	Comments
33	1.8 ± 0.3	18.7 ± 1.0	705 ± 101	OK, ΔP fluctuations
34	1.2 ± 0.1	10.2 ± 0.7	205 ± 71	OK
35	1.2 ± 0.2	10.3 ± 0.6	206 ± 78	OK, ΔP fluctuations
36	1.1 ± 0.2	9.9 ± 0.6	201 ± 71	OK
37	4.1 ± 0.3	7.0 ± 0.5	719 ± 64	OK
38	4.1 ± 0.3	6.9 ± 0.4	692 ± 82	OK
39	4.2 ± 0.3	6.9 ± 0.4	667 ± 67	OK
40	9.6 ± 0.5	6.3 ± 0.5	2376 ± 82	OK
41	9.5 ± 0.5	6.5 ± 0.4	2360 ± 93	OK
42	6.1 ± 0.3	6.3 ± 0.4	1153 ± 68	OK
43	1.9 ± 0.2	29.6 ± 1.9	1184 ± 91	OK
44	1.8 ± 0.3	29.5 ± 2.0	1085 ± 147	OK
45	1.8 ± 0.2	29.6 ± 1.5	1079 ± 104	OK

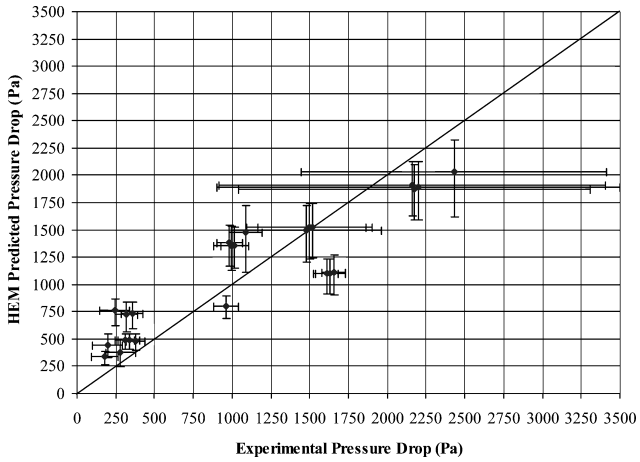

Fig. 12 Large corrugated hose HEM pressure drop vs experimental pressure drop.

where f_{TP} is the two-phase friction factor, G is mass flux, and ρ_m is mixture density. Mixture density is calculated with

$$\frac{1}{\rho_m} = \frac{\dot{m}_L v_L + \dot{m}_V v_V}{\dot{m}_L + \dot{m}_V} \tag{7}$$

where $\dot{m}_L$ is the liquid mass flow rate, $\dot{m}_V$ is the vapor mass flow rate, and v_L and v_V are the liquid and vapor specific volumes, respectively. The two-phase friction factor is typically obtained from the equation

$$f_{TP} = f_{LO}(\mu_{TP}/\mu_L)^{0.25} \tag{8}$$

where f_{LO} is friction factor for all liquid flow, μ_L is liquid dynamic viscosity, and μ_{TP} is the two-phase mixture viscosity. This two-phase mixture viscosity must also be estimated. A commonly used equation by McAdams is

$$1/\mu_{TP} = x/\mu_V + (1-x)/\mu_L \tag{9}$$

where μ_L and μ_V are liquid and vapor dynamic viscosities and x is the flow quality.

Figure 12 shows the predicted and experimental two-phase pressure drop through the large corrugated flexible tube. The horizontal error bars are the combined error shown in the tables. The vertical error bars are computed using the HEM with the mass flow rate error added or subtracted from the mass flow rates. The points with the large horizontal error bars have a very large standard deviation in the pressure-drop measurement. The experimentally measured, single-phase liquid friction factor from the large corrugated hose ground tests was used in the HEM prediction. This method yields surprisingly good results for zero-gravity two-phase flow. The method slightly overpredicts the pressure drop at low pressure drops and slightly underpredicts at higher pressure drops. The average error between the predicted and measured values is 35%. Figure 13 shows the predicted and experimental two-phase pressure drop through the small corrugated flexible tube. Because no single-phase testing is available for the small corrugated hose, a friction factor computed for the large corrugated hose is used in the HEM. In Fig. 11, the plot of single-phase liquid friction factor vs mass flow rate, the large corrugated hose seems to come to equilibrium at a friction factor of 0.11. Because the small corrugated hose has high Reynolds numbers relative to the large flexible tube, the value of 0.11 was chosen as the best approximation. Again, the prediction method yields results quite close to those measured. It is seen that the high pressure drops are again under predicted by the method; however, the average differential error is 11%.

Quick-Disconnect Orifice Model

Figure 14 shows the pressure drop plot for the quick-disconnect apparatus and indicates that modeling the pressure drop through this section as a simple friction factor effect does not work well.

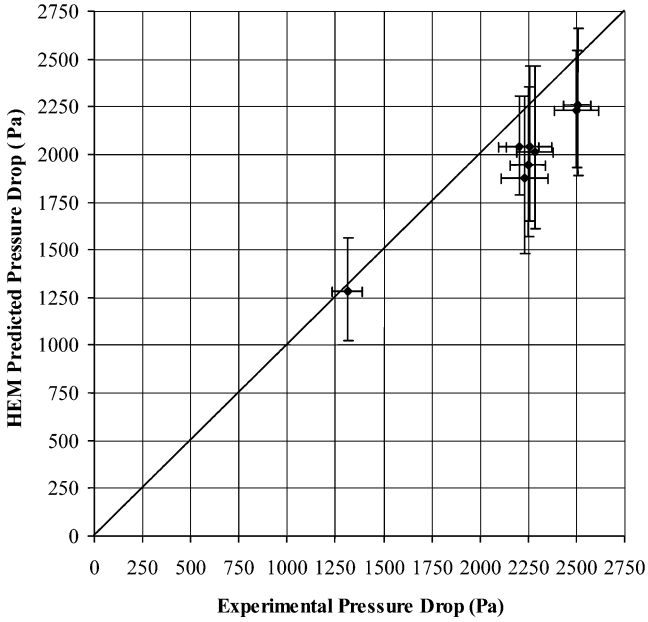

Fig. 13 Small corrugated hose HEM predicted pressure drop vs experimental pressure drop.

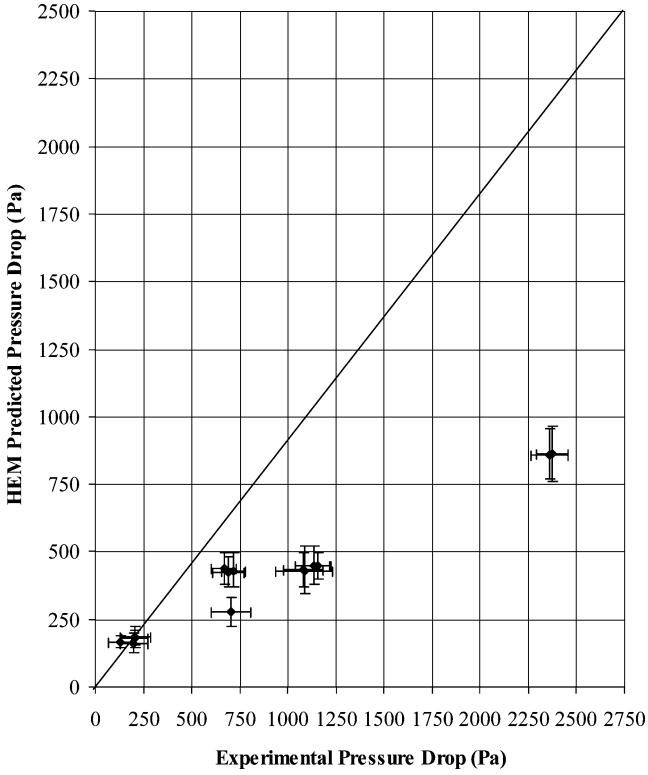

Fig. 14 Quick-disconnect HEM predicted pressure drop vs experimental pressure drop.

The HEM method, Eqs. (6–9), significantly underpredicts the measured pressure drop by a larger and larger amount as pressure drop increases. The average error is 59%. Figure 15 shows the predicted pressure drop for the quick-disconnect when the whole section is modeled as a single, extended orifice using the Chisholm method.

Chisholm's method is

$$\Delta P_{TP}/\Delta P_L = 1 + C\sqrt{\Delta P_V/\Delta P_L} + \Delta P_V/\Delta P_L \tag{10}$$

where $C = Z + (1/Z)$, with $z \cong \sqrt{(\rho_L/\rho_V)}$.

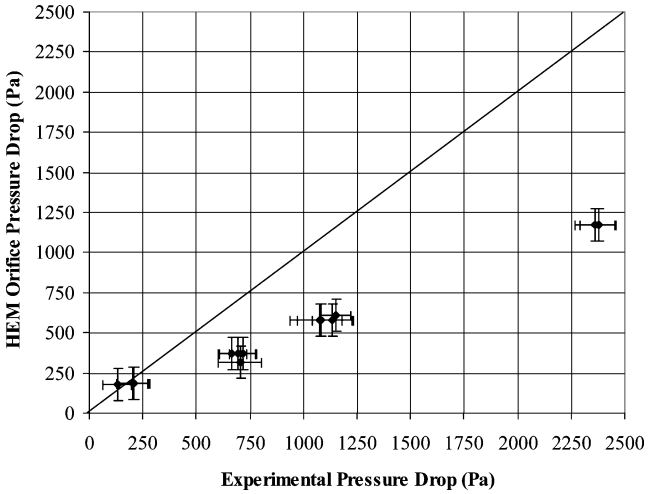

Fig. 15 Quick-disconnect orifice predicted pressure drop vs experimental pressure drop.

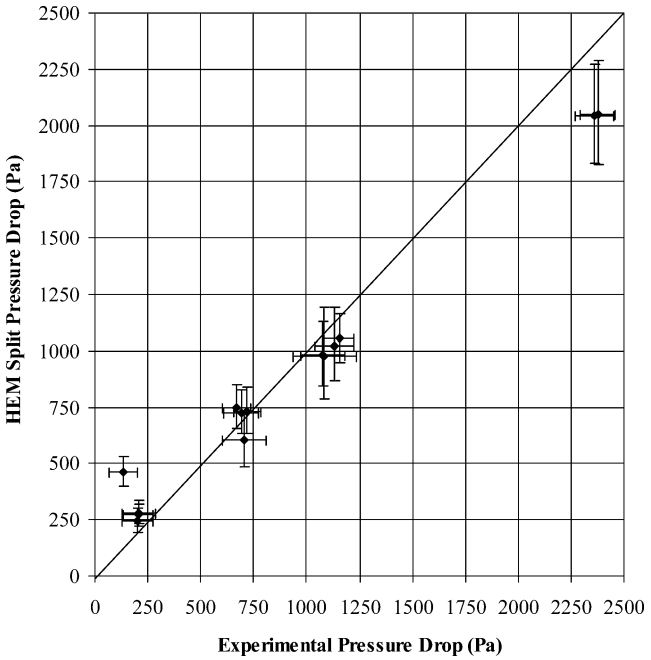

Fig. 16 Quick-disconnect split HEM vs experimental pressure drop.

For this plot, the single-phase ground tests with the quick-disconnect section were interpolated to obtain ΔP_V and ΔP_L in the Chisholm method. It is seen that this method also underpredicts the measured pressure drop as well and has an average differential error of 113%. Further, the error increases significantly as pressure drop increases.

Quick-Disconnect Split-Component Method

Figure 16 is a plot of predicted pressure drop for the quick-disconnect section where the components have been modeled as separate entities, each with its own friction factor. The medium corrugated hose section uses the large corrugated hose friction factor, the smooth glass tube is modeled with the Blasius equation, and the quick disconnect is modeled as an orifice using Chisholm's method. In the preceding section, the single-phase pressure drop through the whole component was used. Now, we are interested in the pressure drops through the quick-disconnect prototype alone. These are unknown and must be estimated.

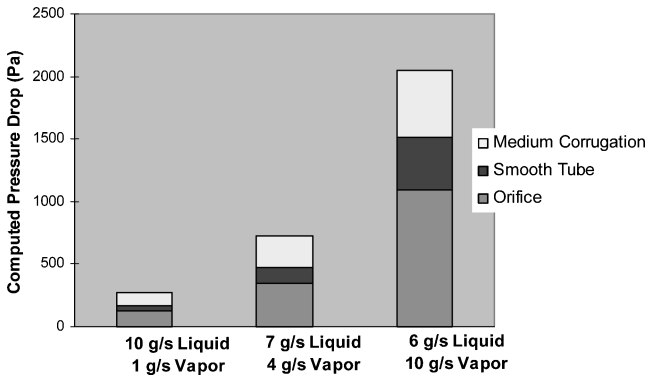

Fig. 17 Contribution from split pieces of quick-disconnect component.

The typical pressure drop equation is of the form

$$\Delta P = K_L(\rho V^2/2) \tag{11}$$

where ΔP is the pressure drop with single-phase liquid or vapor and K_L is the loss coefficient.

Because the loss coefficient for the prototype is unknown, K_L was changed until the overall pressure-drop prediction best matched the experimental results. The loss coefficient was found to be optimum at $K_L = 3$. Figure 16 shows that this method yields good results. The average error is 21%.

Figure 17 shows the contribution to overall predicted pressure drop from each of the split components. It is seen that the orifice is the largest pressure drop, followed in importance by the medium corrugated hose. The relative contribution of each is relatively constant for the three parabolas shown. These three parabolas were chosen to span the pressure drop and mass flow rate range.

Corrugated Hose Friction Factors

Because the two-phase pressure drops through the corrugated hoses can be predicted using the single-phase friction factors, it would be fortuitous if the single-phase friction factors could also be predicted. Because the corrugations are deep and narrow, it is expected that only a fraction of the corrugation depth actually affects the flow. Two approaches were examined to determine if a simple friction factor prediction method existed. The Prandtl boundary-layer thickness δ was calculated for the large flexible tube. This was done to develop a rough estimate of the size of eddies that might be interacting with the corrugations. The equation for δ is

$$\delta = 5L/\sqrt{Re} \tag{12}$$

where L is the horizontal distance. In this case, the pitch of the large corrugated hose, 3.6 mm, was used.[26] For this distance, the boundary-layer thickness is 0.33 mm and 0.18 mm for liquid flows with Reynolds numbers of 3×10^3 and 10^3 respectively. For the large corrugated hose, if eddies were capable of penetrating approximately 0.33 mm into the corrugation, this would provide an ε/D ratio near 0.002. This is approximately an order of magnitude below the single-phase pressure drops measured from the large corrugated hose. An alternative method is to make the assumption that the largest eddy penetrating into a corrugation will have a diameter equal to the width of the corrugation. Although the pitch is 3.6 mm, because of the shape of the corrugations, the corrugation channel is really only about half of that thickness. An ε/D ratio is then calculated from these numbers and used in the Colebrook equation. The friction factors calculated by this method and the boundary-layer thickness method are well below those experimentally determined. The next level of modeling refinement would be to use a computational-fluid-dynamics code to learn how the flow interacts with the narrow, deep corrugations. Then the extent of the flow interaction could be better understood and predicted.

Summary

Conclusions

A series of experiments was conducted using an R12 two-phase flow package under normal reduced-gravity conditions. Single-phase and two-phase data were recorded. The data consisted of liquid and vapor mass flow, triaxial acceleration, and component pressure drop for both ground and flight testing. Three components were tested: two corrugated flexible hose sections 125 cm in length and a quick disconnect. The large and small corrugated hoses had minimum inner diameters of 1.37 and 0.77 cm, respectively. The third component was a combination of smooth stainless-steel tube, a quick-disconnect prototype, medium diameter corrugated flexible hose, and a smooth glass tube. The two-phase flow package was flown on the NASA Johnson Space Center KC-135, which produces approximately 20 s of reduced gravity characterized by accelerations on the order of hundredths of g.

Results from the study include the following: 1) validated and verified single-phase pressure drop data for corrugated hose and quick-disconnect components; 2) validated and verified 0-g two-phase flow pressure-drop data for corrugated hose and quick-disconnect components; 3) single-phase friction factors for corrugated hose and quick disconnect; and 4) a predictive model for 0-g two-phase flow pressure drop using single-phase pressure drop measurements from 1 g.

Experimental data from reduced-gravity aircraft testing must be corrected to account for the aircraft environment effects on the instruments including residual accelerations during the low-gravity period. The pressure data are corrected for instrument effects and test fluid hydrostatic head from small accelerations in the tube axis direction. After corrections are made to measured data, criteria to determine if data were in equilibrium were developed. Data not reaching equilibrium were eliminated from consideration.

Single-phase ground data were used to determine friction factors for the large corrugated hose and quick-disconnect components. These single-phase friction factors were then used in the homogeneous equilibrium model (HEM) to determine the two-phase pressure drops. Because no single-phase data for the small corrugated hose exist, data from the large corrugated hose were used to develop two-phase friction factor and shown to have good agreement. The values of ε/D are quite large because of the disturbance produced in the boundary layer by the components. It is not expected that the procedure could be applied to smaller values of ε/D. For the range of quality tested (0.07 to 0.54 for the large corrugated tubing and 0.12 to 0.25 for the small corrugated tubing), a slight underprediction of ΔP was observed at increasing quality.

The quick-disconnect component experimental data did not match well with the HEM predicted pressure drop. Predictions were made with the Chisholm orifice method where the entire component was modeled as an extended orifice; however, this method, like the HEM, under predicted the data. A more exact method that modeled the quick disconnect as three separate pieces was implemented: a length of smooth tube, a section of corrugated hose, and an orifice. The Blasius equation was used for the single-phase friction factors in the smooth section, and the single-phase ground data from the large corrugated hose used for the corrugated hose. An optimum loss coefficient was determined for the orifice. This method was found to predict the experimental data very well. Modeling the quick disconnect as split sections and using the HEM prediction for the corrugated flexible hoses provides good predictions of 0-g two-phase pressure drop using single-phase, 1-g data. R-12 and other refrigerants are typical of life-support systems; however, this approach could readily be utilized for other fluids including liquid metals. This is an attractive approach because of the difficulty in testing liquid metals in a low-gravity environment. This could be very valuable in cost savings and increased reliability of two-phase space systems using only inexpensive ground testing.

Recommendations

The present study showed that relatively simple methods effectively modeled the pressure drops through the components. However the pressure-drop behavior through the components would be better understood with more ground-testing data. Also, a thorough evaluation of the pressure paddle region where test section two is connected to the package would be very helpful for the analysis conducted in this thesis, as well as several others conducted with data from this experiment package.

Acknowledgments

The authors would like to thank Kathyrn Miller-Hurlbert and John Dezenitis and the Crew and Thermal Systems and Power and Propulsion divisions at NASA Johnson Space Center for funding the experiment that obtained the data as well as Wayne Hill and Foster Miller, Inc., for use of a state-of-the-art two-phase flow experiment. In addition, the authors must thank Igor Carron, Thomas Reinarts, and Monty Wheeler of the Interphase Transport Phenomena group at Texas A&M for collection of the data and for their patient answers to myriad questions.

References

[1]Carbajo, J. J., Yoder, G. L., Qualls, A. L., and Kim, S. H., "Evaluation of Computer Programs for Small Rankine Power Conversion Systems," *Proceedings of the Conference on Applications of Thermophysics in Microgravity and Breakthrough Propulsion Physics*, Springer, Secaucus, NJ, 2004.

[2]Newhouse, A., "Forum on Concepts and Approaches for Jupiter Icy Moons Orbiter Science Capabilities & Workshop Goals," Forum on Concepts and Approaches for Jupiter Icy Moons Orbiter, Lunar and Planetary Institute, June 2003.

[3]Crowley, C. J., and Sam, R. G., "Microgravity Experiments with a Simple Two-Phase Thermal System," Phillips Labo. Directorate of Space Technologies, PL-TR-91-1059, Albuquerque, NM, 1991.

[4]Reitz, J. G., "Zero Gravity Mercury Condensing Research," Thompson Ramo Wooldridge, Inc., 1960.

[5]Koestel, A., and Gutstein, M. V., "Study of Wetting and Nonwetting Mercury Condensing Pressure Drops," NASA-TN-D-2514, 1964.

[6]Lancet, R. T., Abramson, P., and Forslund, R. P., "The Fluid Mechanics of Condensing Mercury in a Low-Gravity Environment," USAF/Lockheed Missiles and Space Co., 1965.

[7]Albers, J. A., and Macosko, R. P., "Experimental Pressure Drop Investigation of Nonwetting Condensing Flow of Mercury Vapor in a Constant Diameter Tube in 1-g and Zero-Gravity Environments," NASA-TN-D-2838, 1965.

[8]Albers, J. A., and Macosko, R. P., "Condensing Pressure Drop of Nonwetting Mercury in a Uniform Tapered Tube in 1-g and Zero-Gravity Environments," NASA-TN-D-3185, 1966.

[9]Albers, J. A., and Namkoong, D., "An Experimental Study of the Condensing Characteristics of Mercury Vapor in Single Tubes," NASA Lewis Research Center, 1964.

[10]Heppner, D., King, D., and Littles, J., "Zero-G Experiments in Two-Phase Fluids Flow Regimes," *Proceedings of the Intersociety Conference on Environmental Systems*, 1975.

[11]Hill, D., Downing, R. S., Rogers, D., Teske, D., and Niggeman, R. E., "A Study of Two-Phase Flow in a Reduced Gravity Environment," Sundstrand Energy Systems, NAS9-17195-T-1884, 1987.

[12]Chen, I., Downing, R. S., Keshock, E., and Al-Sharif, M., "An Experimental Study and Prediction of a Two-Phase Pressure Drop in Microgravity," AIAA Paper 89-74, Jan. 1989.

[13]Lambert, A., "KC-135 Zero Gravity Two Phase Flow Pressure Drop Experiments and Modeling, Master Thesis, Dept. of Nuclear Engineering, Texas A&M Univ., College Station, TX, 1990.

[14]Marsden, K., and Best, F. R., "Vertical Acceleration Conditions in the NASA KC-135," Society of Automotive Engineers, Paper 932299, July 1993.

[15]Hill, W. S., and Best, F. R., "Definition of Two Phase Flow Behaviors for Spacecraft Design," AFK-0062-FM-8933-418, Dept. of Nuclear Engineering, 1990.

[16]Wheeler, M., "An Experimental and Analytical Study of Annular Two Phase Flow Friciton Pressure Drop in a Reduced Acceleration Field," Master's Thesis, Dept. of Nuclear Engineering, Texas A&M Univ., College Station, TX, 1992.

[17]Reinarts, T., "Adiabatic Two Phase Flow Regime Data and Modeling for Zero and Reduced (Horizontal Flow) Acceleration Fields," Ph.D. Dissertation, Dept. of Nuclear Engineering, Texas A&M Univ., College Station, TX, 1993.

[18]Miller, K., Ungar, E., Dzenitis, J., and Wheeler, M., "Microgravity Two-Phase Pressure Drop Data in Smooth Tubing," *Fluid Mechanics Phenomena in Microgravity*, AMD-Vol. 174/FED-Vol. 175, American Society of Mechanical Engineers, 1993.

[19]Nishikawa, K., Sekoguchi, K., Nakasatomi, M., and Kaneuzi, A., "Two-Phase Annular Flow in a Smooth Tube and Grooved Tubes," International Symposium on Research in Cocurrent Gas-Liquid Flow, Sept. 1968.

[20]Chen, I., Bryant, M., Sifuentes, R., and Brady, T., "Two-Phase Ammonia Pressure Drop in Straight Tubes and Flexible Hose," National Heat Transfer Conference, Aug. 1993.

[21]Chisholm, D., "Pressure Gradients During the Flow of Incompressible Two-Phase Mixtures Through Pipes, Venturis and Orifice Plates," *British Chemical Engineering*, Vol. 12, No. 9, 1967, pp. 1368–1371.

[22]Marsden, K., "Two-Phase Friction Pressure Drop Through Corrugated Tubes and Quick Disconnect Attachments in Reduced Gravity," Master's Thesis, Dept. of Mechanical Engineering, Texas A&M Univ., College Station, TX, 1996.

[23]Best, F. R., and Wheeler, M., "Differential Pressure Detector KC-135 Flight Tests of April 9-10, 1991," Texas A&M Univ./NASA Johnson Space Center, June 1991.

[24]Best, F. R., and Wheeler, M., "Paddle Wheel Liquid Flowmeter KC-135 Flight Test of June 18, 1991," Texas A&M Univ./NASA Johnson Space Center, June 1991.

[25]Daugherty, R. L., and Franzini, J. B., *Fluid Mechanics with Engineering Applications*, McGraw–Hill, New York, 1977.

[26]Munson, B. R., Young, D. F., and Okiishi, T. H., *Fundamentals of Fluid Mechanics*, Wiley, New York, 1990.